AIAA JOURNAL
Vol. 31, No. 7, July 1993

Nonlinear Relaxation Navier-Stokes Solver for Three-Dimensional, High-Speed Internal Flows

Jack R. Edwards* and D. Scott McRae†
North Carolina State University, Raleigh, North Carolina 27695

An efficient implicit Navier-Stokes method for computing steady, three-dimensional flowfields characteristic of high-speed propulsion systems is presented. A nonlinear iteration strategy based on planar Gauss-Seidel sweeps is used to drive the solution toward a steady state, with approximate factorization errors within a crossflow plane reduced by the application of a quasi-Newton technique. A hybrid discretization approach is employed, with flux-vector splitting used in the streamwise direction and central differences with artificial dissipation used for the transverse fluxes. Convergence histories and comparisons with experimental data are presented for several three-dimensional shock/boundary-layer interactions. Turbulent closure is provided by a modification of the Baldwin-Barth one-equation model. For the problems considered (206,000–335,000 mesh points), the algorithm provides steady-state convergence in 900–1700 CPU s on a single processor of a Cray Y-MP.

Introduction

PROPULSION system flowfields for high-speed aerospace configurations are often characterized by strong interactions between a shock-dominated inviscid core flow and multiple near-wall viscous regions. To account for such strong viscid/inviscid coupling, propulsion system design, analysis, and optimization methods based on full three-dimensional solutions of the compressible Navier-Stokes equations should be used. Unfortunately, detailed Navier-Stokes simulations of complex propulsion system flowfields often require extremely long run times, as interacting shock waves, strongly mixed hyperbolic-parabolic-elliptic regions, and high spatial resolution requirements combine to produce a large degree of numerical "stiffness." In this article, an algorithmic approach based on upwind relaxation concepts is considered as a first step in the development of a methodology for efficiently computing such complex, three-dimensional flowfields.

Upwind relaxation techniques have evolved from a realization that the coefficient matrices resulting from the linearization of upwind discretizations are nearly diagonally dominant, allowing the use of implicit operators based on line and planar Gauss-Seidel matrix splittings. Such splittings have larger stability bounds than alternating-direction-implicit (ADI) methods, and for two-dimensional, strongly compressible flows, impressive rates of convergence have been achieved.[1,2] Extensions of the upwind relaxation methodology to three dimensions have been reported by Newsome et al.,[3] MacCormack,[4] and Zha and Bilgen[5] for the Navier-Stokes equations and by Thomas et al.,[6] among others, for the Euler equations. In these approaches, forward-backward relaxation in one direction is combined with a planar matrix inversion procedure in the other two directions to provide a solution update. Line Gauss-Seidel or ADI methods are normally used to approximate the planar inversion, since direct techniques are often too expensive. Unconditional stability, a property of some two-dimensional upwind relaxation techniques, is rarely seen in the three-dimensional extensions due to ADI factorization errors within the planar inversions or to a spatially inconsistent linearization of the discretized equation set. If Gauss-Seidel methods are used in the planar inversion, as in the work of Zha and Bilgen[5] and Candler and MacCormack,[7] a high degree of stability may be maintained, but full vectorization of the procedure is inhibited due to necessary recursions.

As a result of the factors just mentioned and inherent coding complexities, three-dimensional upwind relaxation techniques have not enjoyed the success of their two-dimensional counterparts in providing rapid (in terms of CPU time) steady-state convergence. The purpose of this paper is to present an upwind relaxation technique for the three-dimensional Reynolds-averaged Navier-Stokes equations that eliminates many of the weaknesses of earlier approaches. In particular, the new algorithm is fully implicit and fully vectorizable, requires only planar matrix storage, and is capable of sustaining a high convergence rate. Based on an extension of the two-dimensional nonlinear relaxation method of Edwards and McRae[8] to three dimensions, the algorithm incorporates a hybrid upwind/central-differencing strategy that can be linearized in a spatially consistent manner. A high degree of information propagation is achieved through the use of a stable, fully coupled sequence of planar Gauss-Seidel sweeps enhanced by a two level residual updating procedure. Planar matrix inversions are stabilized by the application of a quasi-Newton iterative method.

Validation cases for the algorithm are taken primarily from the current literature on three-dimensional turbulent shock/boundary-layer interactions, since these phenomena dominate the flow physics within the configurations of interest. A case involving the Mach 4 interaction of a turbulent boundary layer with a sharp fin is presented.[9,10] Also, a computation of a three-dimensional crossing shock/turbulent-boundary-layer interaction generated by two symmetric sharp fins is shown.[11–13] Finally, a simulation of a Mach 4 laminar flow into a ramped duct with a sidewall is considered as a "model problem" for an inlet flowfield. Turbulent effects are simulated by a modification of the one-equation model of Baldwin and Barth,[14] and all cases presented include comparisons with experimental data and convergence histories.

Governing Equations and Their Discretization

The flowfields under consideration are governed by the three-dimensional, compressible, Reynolds-averaged Navier-Stokes equations. In a curvilinear coordinate system defined

Received Sept. 3, 1992; based in part on Paper 93-0540 presented at the AIAA 31st Aerospace Sciences Meeting, Reno, NV, Jan. 11–14, 1993; revision received Jan. 12, 1993; accepted for publication Jan. 13, 1993.

*Visiting Assistant Professor, Department of Mechanical and Aerospace Engineering; currently at Department of Mechanical Engineering, North Carolina A&T State University, Greensboro, NC 27411. Member AIAA.

†Associate Professor, Department of Mechanical and Aerospace Engineering, Campus Box 7910. Member AIAA.

by the steady transformation $\xi = \xi(x, y, z)$, $\eta = \eta(x, y, z)$, and $\zeta = \zeta(x, y, z)$, a thin-layer approximation to the Navier-Stokes equations can be written in nondimensionalized strong conservation law form as

$$\frac{\partial \hat{U}}{\partial t} + \frac{\partial \hat{E}}{\partial \xi} + \frac{\partial \hat{F}}{\partial \eta} + \frac{\partial \hat{G}}{\partial \zeta} = \frac{1}{Re}\left(\frac{\partial \hat{R}}{\partial \eta} + \frac{\partial \hat{S}}{\partial \zeta}\right) \tag{1}$$

where $\hat{U}$ is the vector of conserved variables; $\hat{E}$, $\hat{F}$, and $\hat{G}$ are the inviscid fluxes; and $\hat{R}$ and $\hat{S}$ are the thin-layer viscous fluxes in the η and ζ directions. The Reynolds number is denoted by Re, and the quantity J will be used to represent the Jacobian of the Cartesian-to-curvilinear transformation.

The convective and pressure terms in Eq. (1) are represented as a flux balance over a mesh cell using Van Leer's flux-vector splitting in the primary flow direction ξ and central differencing with flux-limited artificial dissipation in the secondary flow directions η and ζ. Consider the following difference representation of $\partial \hat{E}/\partial \xi$:

$$\frac{1}{\Delta \xi}\left(\tilde{E}_{i+\frac{1}{2}} - \tilde{E}_{i-\frac{1}{2}}\right) \tag{2}$$

where $\tilde{E}_{i+\frac{1}{2}}$ is a function of the split fluxes $\hat{E} = \hat{E}^+ + \hat{E}^-$ and is defined as

$$\tilde{E}_{i+\frac{1}{2}} = \hat{E}^+_{i+\frac{1}{2}}(\tilde{W}_L) + \hat{E}^-_{i+\frac{1}{2}}(\tilde{W}_R) \tag{3}$$

In the previous expression, the $i + \frac{1}{2}$ subscript denotes the evaluation of the transformation metrics at the cell interface between i and $i + 1$, and $\tilde{W}_L$ and $\tilde{W}_R$ correspond to interpolations of the primitive variable vector $\tilde{W} = [\rho, u, v, w, p]^T$ to the $i + \frac{1}{2}$ interface:

$$\tilde{W}_R = \tilde{W}_{i+1} - \frac{\Phi_{i+3/2}}{2}\left[(1-\kappa)\Delta\tilde{W}_{i+3/2} + (1+\kappa)\Delta\tilde{W}_{i+\frac{1}{2}}\right] \tag{4}$$

$$\tilde{W}_L = \tilde{W}_i + \frac{\Phi_{i-\frac{1}{2}}}{2}\left[(1-\kappa)\Delta\tilde{W}_{i-\frac{1}{2}} + (1+\kappa)\Delta\tilde{W}_{i+\frac{1}{2}}\right]$$
$$\Delta\tilde{W}_{i+\frac{1}{2}} = \tilde{W}_{i+1} - \tilde{W}_i \tag{5}$$

The function Φ is a pressure-based flux-limiting operator that is designed to reduce the interpolation to first-order accuracy in regions of large gradient in the solution:

$$\Phi_{i+\frac{1}{2}} = \max\left(0, \frac{1}{2} - \frac{|p_{i+1} - p_i|}{|p_{i+1}| + |p_i|}\right) \tag{6}$$

For the transverse derivative $\partial \hat{F}/\partial \eta$, the numerical flux function used in the control volume approach is

$$\tilde{F}_{j+\frac{1}{2}} = \tfrac{1}{2}[\hat{F}_{j+\frac{1}{2}}(\tilde{W}_j) + \hat{F}_{j+\frac{1}{2}}(\tilde{W}_{j+1}) - d_{j+\frac{1}{2}}] \tag{7}$$

where the dissipation operator $d_{j+\frac{1}{2}}$ is given by

$$d_{j+\frac{1}{2}} = \Psi_{j+\frac{1}{2}}|\lambda_{j+\frac{1}{2}}|(U_R - U_L)_{j+\frac{1}{2}}$$

The notations U_R and U_L represent the evaluation of the force vector $U = J\hat{U}$ at the $j + \frac{1}{2}$ interface using transversely oriented interpolations of the forms shown in Eqs. (4) and (5). The quantities $\Psi_{j+\frac{1}{2}}$ and $|\lambda_{j+\frac{1}{2}}|$ represent, respectively, a pressure sensor designed to add dissipation at extrema of the solution and the magnitude of the spectral radius of the transverse flux Jacobian evaluated at the $j + \frac{1}{2}$ cell interface. In particular,

$$\Psi_{j+\frac{1}{2}} = c_0 + c_1 \min[1, \max(v_j, v_{j+1})] \tag{8}$$

where

$$v_j = \frac{|p_{j+1} - 2p_j + p_{j-1}|}{p_j}$$

and

$$|\lambda_{j+\frac{1}{2}}| = \left(\frac{|V_c| + a\sqrt{\eta_x^2 + \eta_y^2 + \eta_z^2}}{J}\right)_{j+\frac{1}{2}} \tag{9}$$

where a is the speed of sound and V_c is the contravariant velocity component in the η direction.

Values of the dissipation/interpolation constants used in this investigation are the following: $\kappa = 0$ (Fromm's scheme), $c_0 = 0.1$, and $c_1 = 1.0$. A similar form for the $\partial \hat{G}/\partial \zeta$ flux derivative is adopted, and the stress term vectors $\partial \hat{R}/\partial \eta$ and $\partial \hat{S}/\partial \zeta$ are discretized using second-order central differences.

Linearization

The residual vector $\mathcal{R}$ is formed from a natural ordering of the discretized approximation to Eq. (1) over the mesh nodes. As the solution approaches a steady state, the residual vector approaches zero. At time level n, a backward Euler time linearization of the difference approximations to the inviscid fluxes yields a linear system of the form

$$\left(\frac{M}{J\Delta t} + \delta_\xi^- A^+ + \delta_\xi^+ A^- + \delta_\eta B + \delta_\zeta C\right)^n \delta W^{n+1} = -\mathcal{R}^n \tag{10}$$

where $M = \partial U/\partial W$, δW^{n+1} is the update vector $W^{n+1} - W^n$, and the matrices $A^\pm$, B, and C are the flux Jacobians. The vector W is composed of the primitive variables ρ, u, v, w, and e, and the flux Jacobians at a particular grid point are differenced as

$$\delta_\xi^- A^+ + \delta_\xi^+ A^- = \frac{1}{2\Delta\xi}(3A_i^+ - 4A_{i-1}^+ + A_{i-2}^+)$$
$$- \frac{1}{2\Delta\xi}(3A_i^- - 4A_{i+1}^- + A_{i+2}^-) \tag{11}$$

$$\delta_\eta B = \frac{1}{2\Delta\eta}(B_{j+1} - B_{j-1}) \tag{12}$$

$$\delta_\zeta C = \frac{1}{2\Delta\zeta}(C_{k+1} - C_{k-1}) \tag{13}$$

This linearization, although not exact, is second-order accurate in space, thus providing a proper match of the implicit and explicit operators. Because of the central differencing of the transverse Jacobians (η and ζ), however, only the $M/J\Delta t$ and $(3/2\Delta\xi)(A_i^+ - A_i^-)$ terms contribute to the diagonal elements of the linear system, Eq. (10). The addition of diffusion-like terms formed by the approximate linearization of the thin-layer viscous fluxes and the η and ζ dissipation model provides some diagonal enhancement.

An expression for the linearization of the thin-layer flux derivatives can be obtained analytically by assuming constant viscosities and using a Taylor expansion of the required derivatives.[15] The result for the η thin-layer term is given as

$$\delta_\eta\left(\frac{\partial \hat{R}}{\partial W}\right)\delta W^{n+1} = \delta_\eta^2\left(\frac{\partial \hat{R}}{\partial W_\eta}\,\delta W^{n+1}\right) \tag{14}$$

where W_η is the vector $[\rho_\eta, u_\eta, v_\eta, w_\eta, e_\eta]^T$, and the δ_η^2 operator represents a finite differenced second derivative. The actual computation of this relation at every point in the domain is expensive, and a simpler alternative is found by replacing the matrix $\partial \hat{R}/\partial W_\eta$ with its spectral radius times the identity matrix.[15] A straightforward eigenvalue calculation gives the required spectral radius (for linearization in terms of W) as

$$\sigma_\eta^{\hat{R}} = \frac{\gamma}{JRe}\left(\frac{\mu}{Pr} + \frac{\mu_t}{Pr_t}\right)(\eta_x^2 + \eta_y^2 + \eta_z^2) \tag{15}$$

where Pr and Pr_t are the laminar and turbulent Prandtl numbers. A similar expression for the linearization of the dissipa-

tion model is determined by assuming Ψ and λ to be locally constant and U_L and U_R to be first-order interpolations. For the η direction, the linearization is given by

$$\delta_\eta\left(\frac{\partial d}{\partial W}\right)\delta W^{n+1} = \delta_\eta^2(\Psi|\lambda|M\delta W^{n+1}) \tag{16}$$

For convenience, the matrix formed by the addition of the thin-layer and artificial dissipation elements of Eqs. (14) and (16) to the left-hand side of Eq. (10) will be denoted as $\bar{A}$.

Relaxation Procedure

Given an exact linearization, the exact solution of $\bar{A}^n\delta W^{n+1} = -\mathcal{R}^n$ would approximate a Newton step for large Δt, and quadratic convergence to the steady state could eventually be obtained. Direct factorization procedures for $\bar{A}$ are impractical for large problems, and most researchers advocate the splitting of $\bar{A}$ into products of easily inverted operators, whose action on the residual vector produces a solution update. The method presented in this work is an extension of the nonlinear relaxation algorithm of Edwards and McRae[8] to three dimensions. The basic two-dimensional approach, described in Ref. 8, combines the best features of a "linear" line Gauss-Seidel iteration[2,16] and a more "nonlinear" relaxation method.[1]

In the three-dimensional extension, a plane-based partitioning of $\bar{A}$ is defined by denoting the matrices corresponding to a constant ξ plane

$$\left[\frac{M}{J\Delta t} + \frac{3}{2\Delta\xi}(A^+ - A^-) + \delta_\eta\hat{B} + \delta_\zeta\hat{C}\right]_i$$

by D and letting L and U be block triangular matrices composed of

$$\left(-\frac{2}{\Delta\xi}A^+_{i-1}, \quad \frac{1}{2\Delta\xi}A^+_{i-2}\right)$$

and

$$\left(\frac{2}{\Delta\xi}A^-_{i+1}, \quad -\frac{1}{2\Delta\xi}A^-_{i+2}\right)$$

respectively. The notations $\hat{B}$ and $\hat{C}$ represent the addition of the approximate linearizations for the viscous fluxes and the dissipation model to the matrix D. With these definitions, the nonlinear relaxation process for the entire matrix at time level n is defined as

$$\begin{aligned}
(D+U)^n\delta W^{n+\frac{1}{2}} &= -\mathcal{R}(W^n) - \omega_f L^{n-\frac{1}{2}}\delta W^n \\
W^{n+\frac{1}{2}} &= W^n + \omega_b\delta W^{n+\frac{1}{2}} \\
(D+L)^{n+\frac{1}{2}}\delta W^{n+1} &= -\mathcal{R}(W^{n+\frac{1}{2}}) - \omega_b U^n\delta W^{n+\frac{1}{2}} \\
W^{n+1} &= W^{n+\frac{1}{2}} + \omega_f\delta W^{n+1}
\end{aligned} \tag{17}$$

At a particular ξ plane, an expansion of the first (backward) sweep in Eq. (17) yields

$$\begin{aligned}
D_i^n\delta W_i^{n+\frac{1}{2}} = -\mathcal{R}(W_i^n) - \Bigg[&\left(\frac{2}{\Delta\xi}A^-_{i+1}\right)^n\delta W_{i+1}^{n+\frac{1}{2}} \\
&- \left(\frac{1}{2\Delta\xi}A^-_{i+2}\right)^n\delta W_{i+2}^{n+\frac{1}{2}}\Bigg] - \omega_f\Bigg[\left(-\frac{2}{\Delta\xi}A^+_{i-1}\right)^{n-\frac{1}{2}}\delta W_{i-1}^n \\
&+ \left(\frac{1}{2\Delta\xi}A^+_{i-2}\right)^{n-\frac{1}{2}}\delta W_{i-2}^n\Bigg]
\end{aligned} \tag{18}$$

The algorithm is implemented by using two arrays to store the matrix-vector products within the square brackets of Eq. (18). The second array is known from the previous sweep, and the first array is computed after the correction $\delta W_{i+1}^{n+\frac{1}{2}}$ is calculated. A similar form for the second (forward) sweep in Eq. (17) holds. The rate of information propagation between sweeps is controlled by the ω_f and ω_b under-relaxation parameters, which can be chosen to maximize the convergence rate for a given problem. Evaluations of the flux Jacobians are only required at a particular ξ plane within a given sweep, making the scheme fairly storage efficient. Note that the update vector δW needs to be set to zero only before the first iteration. Otherwise, the previous update is used as a "forcing function" for the next sweep, a notion that can be further explored by considering the following scenario. If $L^{n-\frac{1}{2}}\delta W^n$ and $U^n\delta W^{n+\frac{1}{2}}$ in Eq. (17) were replaced by $L^n\delta W^{n+\frac{1}{2}}$ and $U^{n+\frac{1}{2}}\delta W^{n+1}$, Eq. (17) would resemble two steps of Newton's method. The use of $L^{n-\frac{1}{2}}\delta W^n$ and $U^n\delta W^{n+\frac{1}{2}}$, evaluated from the *previous* sweeps, seems to make each Gauss-Seidel step approximate a direct inversion of the system Jacobian more closely, and the resulting algorithm should converge faster than more conventional relaxation strategies. Such an improvement in convergence rate has been demonstrated in two dimensions for shock-separated flowfields.[8] In the sections that follow, the degree of convergence rate improvement offered by the three-dimensional extension will be ascertained.

Crossflow Matrix Factorization and Time Stepping

With the planar Gauss-Seidel partitioning of $\bar{A}$, the problem has been reduced to the solution of a sparse, block pentadiagonal linear system,

$$D_i\delta W_i = \text{RHS}(18) \tag{19}$$

at each ξ station where RHS stands for right-hand side. Although direct factorization procedures for D_i are possible, they are time consuming, and a more efficient alternative is given by the ADI factorization of D_i defined as

$$N = (\hat{D} + \delta_\eta\hat{B})\hat{D}^{-1}(\hat{D} + \delta_\zeta\hat{C}) \tag{20}$$

where, for convenience, $\hat{D}$ is defined as $(M/J\Delta t) + (3/2\Delta\xi)(A_i^+ - A_i^-)$ plus the block diagonal components of the viscous flux and dissipation model linearizations. This factorization can be fully vectorized within a constant ξ plane and, for many problems, constitutes a good approximation to D_i. When highly stretched grids in two or more coordinate directions are used, however, small time steps are required to stabilize the ADI factorization, and the overall convergence rate of the relaxation process is thus degraded. A possible way of circumventing this difficulty is to use the ADI factorization N as a preconditioner for an iterative method designed to approximate the actual solution of Eq. (19). For large time steps, however, even this approach may fail unless the iterative method possesses a "bounded deterioration" property. Such a trait, inherent within a linear extension of Broyden's quasi-Newton method,[17] guarantees that errors (or instabilities) due to the preconditioning do not grow as the crossflow iteration progresses.

Reference 8 details some theoretical and practical aspects of the application of various quasi-Newton algorithms to accelerate the convergence of implicit computational fluid dynamics (CFD) schemes. A "pseudocode" implementation is also given in Ref. 8, and only the highlights of the extension to linear systems will be presented in this work. Given an initial approximation to the crossflow plane matrix D_i (N in our case), Broyden's quasi-Newton technique will seek to "improve" N at every crossflow iteration l so that the linear residual

$$\mathcal{F}(\delta W_i^l) = \text{RHS}(18) - D_i\delta W_i^l \tag{21}$$

approaches zero q-superlinearly [$(\|\mathcal{F}^l\|_2/\|\mathcal{F}^{l-1}\|_2) \Rightarrow 0$ as $l \Rightarrow \infty$]. The updating algorithm is based on the Sherman-Morrison-Woodbury theorem[18] and is given by the following relations:

$$\delta V^l = N_l^{-1}\mathcal{F}(\delta W_i^l) \tag{22}$$

$$\delta W_i^{l+1} = \delta W_i^l + \delta V^l \tag{23}$$

$$N_{l+1}^{-1} = (I - \theta_l \psi_l^T) N_l^{-1} \tag{24}$$

where

$$\psi_l = \frac{\delta V^l}{\delta V^l \cdot \delta V^l} \tag{25}$$

$$\theta_l = \frac{N_l^{-1} \mathfrak{F}(\delta W_i^{l+1})}{1 + \psi_l \cdot N_l^{-1} \mathfrak{F}(\delta W_i^{l+1})} \tag{26}$$

and I is the identity matrix. By multiplying Eq. (24) by the updated residual $\mathfrak{F}(\delta W_i^{l+1})$, one arrives at a recursion relation for the new correction δV^{l+1} that requires only vector operations, provided that an initial correction $N_1^{-1}\mathfrak{F}(\delta W_i^{l+1})$ is available. This vector is obtained by the application of the ADI splitting of Eq. (20). The Broyden algorithm can thus be viewed as a "stabilization" process for the ADI factorization, Eq. (20). A computationally efficient implementation of the preceding method requires the storage of $2m$ vectors for θ and ψ, where m is the number of allowable Broyden steps per crossflow plane (four in this work). Storage for the matrix D_i and the factorization N must also be provided.

At the nth nonlinear iteration level, a "global" time step is obtained from the relation

$$\Delta t_0 = \Delta t_{\max} \frac{\|\mathfrak{R}_{\max}\|_2}{\|\mathfrak{R}_n\|_2} \tag{27}$$

where the subscript max indicates evaluation of the quantity at the location of maximum residual norm. The initial value for $\Delta t_{\max}$ is an input parameter, and the time step is only allowed to increase if the residual norm decreases. A geometrically scaled "local" time step is defined by the following point function:

$$\Delta t_{i,j,k} = \Delta t_0 \frac{1}{1 + \sqrt{(J^{-1})_{\text{rms}} J_{i,j,k}}} \tag{28}$$

where $J^{-1} = 1/J$ is a measure of the cell volume and

$$(J^{-1})_{\text{rms}} = \frac{1}{nn} \left[\sum_{i,j,k} (J_{i,j,k}^{-1})^2 \right]^{1/2} \tag{29}$$

The quantity nn is the total number of points in the domain.

Turbulence Model

Reynolds stress effects are simulated using a modified version of the one-equation model of Baldwin and Barth.[14] In this approach, a transport equation for the quantity $F \equiv k^2/\epsilon$ is derived from partially modeled versions of the turbulent kinetic energy (k) and the dissipation rate (ϵ) equations. The eddy viscosity μ_t is obtained from the relation

$$\mu_t = \rho C_\mu F D_1 D_2 \tag{30}$$

where C_μ is a constant and D_1 and D_2 are wall-damping functions of the form

$$D_i = 1 - \exp\left(-\frac{\hat{n}^+}{C_i^+}\right) \tag{31}$$

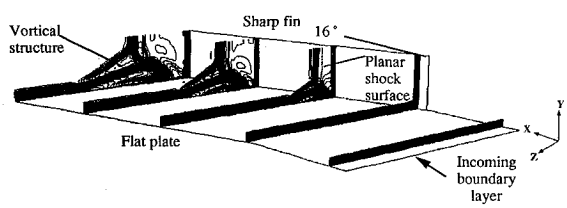

Fig. 1 Pitot pressure contours (Kim case, 16-deg fin).

The transport equation is given by

$$B_1 \rho \frac{DF}{Dt} = B_2 f_2(D_1, D_2) \sqrt{\rho FP} + \frac{1}{Re}\left[\left(\mu + \frac{\mu_t}{\sigma_R}\right)\nabla^2 F - \frac{1}{\sigma_\epsilon}(\nabla \mu_t) \cdot \nabla F\right] \tag{32}$$

where B_1, B_2, σ_R, and σ_ϵ are constants; $f_2(D_1, D_2)$ is another damping function; and

$$P = \mu_t \left[\left(\frac{\partial U_i}{\partial x_j} + \frac{\partial U_j}{\partial x_i}\right)\frac{\partial U_i}{\partial x_j} - \frac{2}{3}\left(\frac{\partial U_k}{\partial x_k}\right)^2 \right]$$

The terms in Eq. (32) represent, respectively, convection, production, diffusion, and destruction of the quantity F. In their paper, Baldwin and Barth present a robust implementation of Eq. (32) that allows for the use of relaxation or ADI techniques to advance the solution for F. Their methodology was closely followed in this work, and the reader is advised to consult Ref. 14 for further details.

Initial tests of the Baldwin-Barth approach for several two-dimensional, supersonic, compression-corner interactions revealed that the model predicts wall pressure distributions and separation point locations quite well but severely overpredicts the extent of axial separation, causing reattachment far downstream of experimentally measured locations. The "destruction" term in Eq. (32) was found to be the primary culprit, and an alternative form for the term was borrowed from the one-equation model of Spalart and Allmaras.[19] With this modification, the transport equation for F becomes

$$B_1 \rho \frac{DF}{Dt} = B_2 f_2(D_1, D_2) \sqrt{\rho FP} + \frac{1}{Re}\left[\frac{1}{\sigma_R}(\mu + \mu_t)\nabla^2 F - \frac{1}{\sigma_\epsilon}\frac{\mu_t F}{\hat{n}^2}\right] \tag{33}$$

with

$$f_2(D_1, D_2) = \left(\frac{1}{\kappa \hat{n}^+} + D_1 D_2\right)\sqrt{D_1 D_2}$$

$$\frac{1}{\sigma_\epsilon} = \frac{B_2 \sqrt{C_\mu}}{\kappa^2}$$

$$\frac{1}{\sigma_R} = 1.64\left(\frac{1}{\sigma_\epsilon}\right)$$

$$B_1 = 1.15$$

$$B_2 = 1.0$$

$$C_1^+ = 18$$

$$C_2^+ = 10$$

$$C_\mu = 0.09$$

$$\kappa = 0.41 \tag{34}$$

Values for the constants B_1, B_2, C_1^+, C_2^+, and σ_R were found by comparing flat plate results with the compressible law-of-the-wall and the outer layer formulation of Cebeci et al.[20] When two or more walls are considered, the normal distance $\hat{n}$ and the corresponding wall coordinate $\hat{n}^+$ are taken to be the minimums of the measured values from each wall. Equation (33) is updated by a planar relaxation technique after the completion of the second sweep in Eq. (17).

Results and Discussion

Test cases for the validation of the algorithm are taken primarily from the current literature on three-dimensional

shock-wave/turbulent boundary-layer interactions. A case involving laminar flow within a three-dimensional ramped-duct geometry is also considered. Results are represented in Figs. 1–10 as comparisons with experimental data, contour plots, and convergence histories. The grids used in the simulations are heavily clustered near the walls to resolve viscous layer gradients, and standard Navier-Stokes boundary conditions are employed. The Baldwin-Barth model requires a wall $\hat{n}^+$ of 2.5–3.0, and this criterion is met more than adequately for the turbulent cases. To indicate convergence behavior, the $\mathcal{L}_2$ norm of the residual vector is plotted vs Cray Y-MP CPU time. For all test cases, convergence rate comparisons are made with a three-dimensional analog of the nonlinear relaxation approach of Thomas and Walters.[1] This algorithm is obtained from Eq. (17) by neglecting the sweep-coupling terms $L^{n-\frac{1}{2}}\delta W^n$ and $U^n\delta W^{n+\frac{1}{2}}$ and setting ω_f and ω_b to unity. The performance of the Thomas and Walters algorithm should be indicative of that obtained by the nonlinear relaxation approaches of Refs. 3 and 6, which involve the updating of the solution and recalculation of the residual vector after the planar matrix inversion at each streamwise location. A first-order Taylor series expansion of the "nonlinear" residuals obtained at each streamwise location within each sweep yields an algorithm equivalent to the approach of Thomas and Walters.

A simulation involving the interaction of a turbulent boundary layer with a sharp fin is presented in Figs. 1–4. This case corresponds to an experiment conducted by Kim et al., [9] for which computational results using Baldwin-Lomax and k-ϵ turbulence models have been presented by Knight et al.[10] Flow conditions are $M_\infty = 3.96$, $T_\infty = 71$ K, and $T_{\text{wall}} = 283$ K, with a freestream Reynolds number per meter of 72.2×10^6. A two-dimensional version of the algorithm[8] was used to generate an inflow turbulent profile. Figure 1 shows pitot pressure contours within the interaction region for a fin angle of 16 deg. The fin-generated oblique shock separates the boundary layer, producing a vortical structure that enlarges in a quasi-conical fashion.[10] The displacement effect of the separated viscous region creates another shock structure that intersects the fin-generated shock. Figures 2 and 3 illustrate surface pressure and skin friction distributions along an arc located at a radius of 8.89 cm from the fin leading edge (the fin length is 12.7 cm). Agreement with experiment is generally good, although the computation underpredicts the pressure decrease resulting from the expansion of the flow around the separation bubble. In general, the computational results indicate an improvement in accuracy over the results presented in Ref. 10. Since the grid distributions are similar, much of the improvement can be attributed to the use of the modified Baldwin-Barth turbulence model.

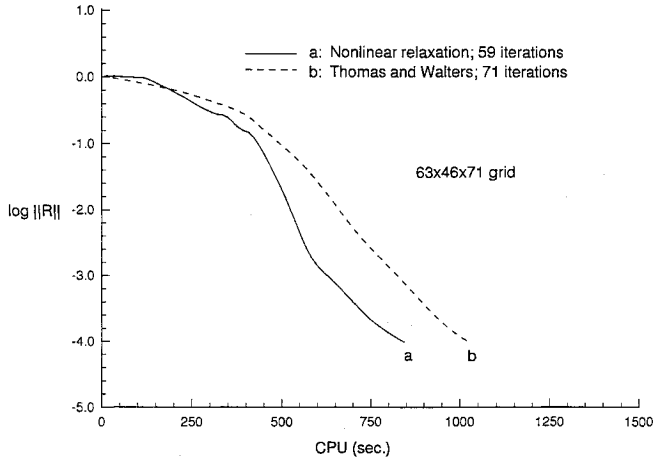

Fig. 4 Convergence histories (Kim case, 16-deg fin).

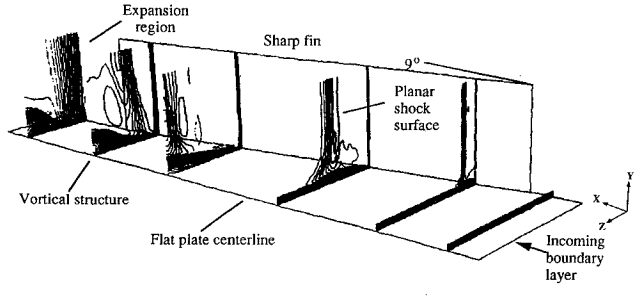

Fig. 5 Pitot pressure contours (Bogdanoff case, 9-deg fin).

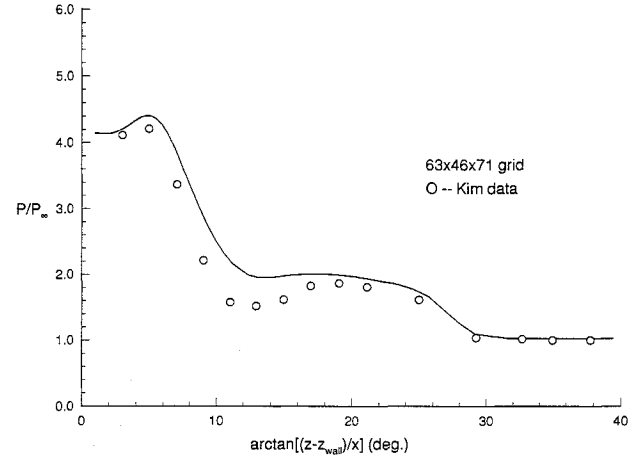

Fig. 2 Wall pressure distribution (Kim case, 16-deg fin).

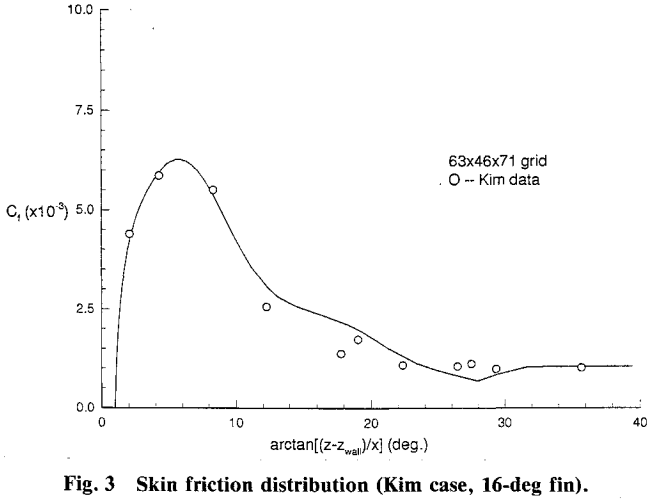

Fig. 3 Skin friction distribution (Kim case, 16-deg fin).

Convergence histories for the simulation (performed on a $63 \times 46 \times 71$ grid) are shown in Figure 4. For these cases and for the crossing shock interaction to be discussed next, the under-relaxation factors ω_f and ω_b were set to unity. The initial and final values for the global time step Δt_0 were 0.015 and 0.1, respectively, and four Broyden iterates per crossflow plane were required to stabilize the factorization. The convergence criterion for this predominately streamwise supersonic flow is met in approximately 840 s of CPU time using the nonlinear relaxation approach of Eq. (17). A modest 18% improvement in performance over that provided by the method of Thomas and Walters (1025 s of CPU time) is achieved.

A simulation of a crossing shock-wave/turbulent boundary-layer interaction generated by two symmetric sharp fins is presented in Figs. 5–8. A fin angle of 9 deg is considered, and the configuration corresponds to an experiment originally conducted by Batcho et al.[11] at the following conditions: $M_\infty = 2.95$, $T_\infty = 97$ K, $T_{\text{wall}} = 247$ K, $Re/\text{m} = 64.3 \times 10^6$, and fin length = 22.86 cm. Recently, Bogdanoff and Stokes[12] have presented a much more complete set of pressure data for this

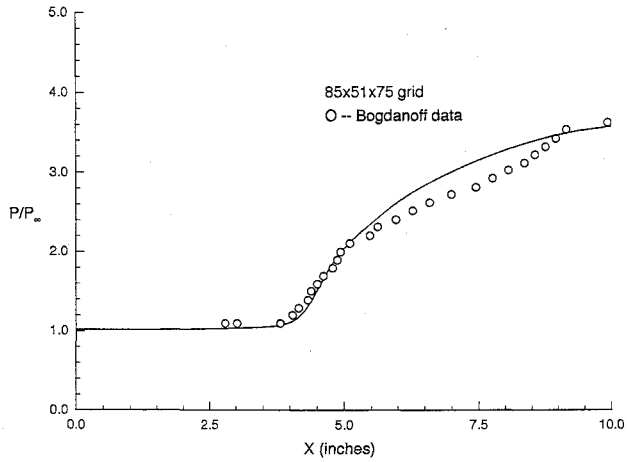

Fig. 6 Centerline pressure distribution (Bogdanoff case, 9-deg fin).

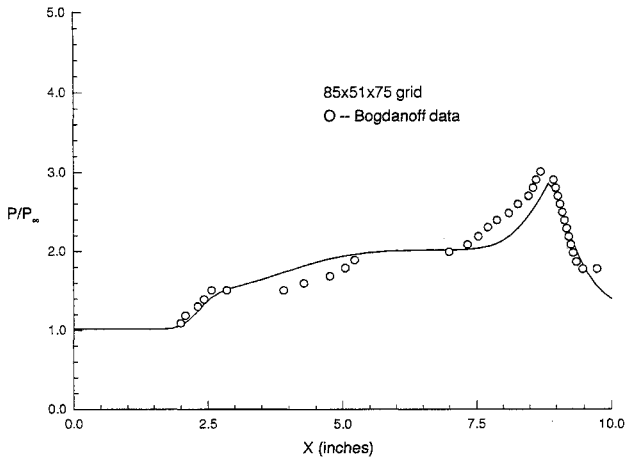

Fig. 7 Pressure distribution (Bogdanoff case, 1.4 in. off centerline).

interaction, albeit at a slightly lower Mach number of 2.93. Detailed descriptions of this flowfield, taken from both computational and experimental points of view, have been presented previously,[12,13,21] and only the highlights will be outlined in this work.

General features of the crossing shock interaction are illustrated in the pitot pressure contours of Fig. 5. Only half of the interaction is actually shown, since centerline symmetry was assumed to reduce gridding requirements. The dominant inviscid features are obviously the crossing planar shock surfaces. Expansion fans generated as the flow spills around the trailing edges of the fins also influence the interaction region. Of particular note is the formation of a large, centerline-oriented vortical structure within the viscous layer downstream of the crossing location. Figure 6 compares the calculated centerline surface pressure distribution with the data of Bogdanoff and Stokes. The upstream extent of the centerline structure is well predicted; however, the algorithm tends to overpredict the pressure level downstream of the crossing location. Similar trends are noted in Fig. 7, which compares computed wall pressures with the experimental data along a line located 1.4 in. inboard (toward the fin) of the centerline.

An $85 \times 51 \times 75$ grid was used to generate the computational data. Curves a and b of Fig. 8 compare the convergence behavior of the nonlinear relaxation approach Eq. (17) and the method of Thomas and Walters for this problem. For these cases, the initial and final values of the global time step were the same as in the sharp fin interaction, and again four Broyden iterates per crossflow plane were used. Equation (17) converges in under 28 min of CPU time (curve a), demonstrating a 35% improvement over the time obtained by the approach of Thomas and Walters (≈ 42 min of CPU time). Curve c of Fig. 8 illustrates the utility of the Broyden approach for stabilizing the crossflow factorization. Without Broyden iterates, the maximum allowable global time step for the algorithm of Thomas and Walters is restricted to 0.029, and although the cost per iteration is decreased by about 30%, the overall time to convergence is increased significantly. It is likely that the use of the Broyden approach would result in even greater improvement if further residual reductions were required.

A Mach 4 laminar flow into a ramped duct with a sidewall is considered as a final test case. Such a simulation provides a model for the complex viscid-inviscid interactions characteristic of three-dimensional supersonic/hypersonic inlet configurations. The top of the duct, an unramped flat plate, extends from $X = 1.27$ to 13.97 and from $Z = 0.0$ to 3.1 (all dimensions in centimeters). The bottom of the duct is of the same dimension but is ramped 10 deg in the X-Y plane, beginning at $X = 7.62$. A straight, vertical sidewall, extending from $X = 0.0$ to 13.97 and from $Y = 0.0$ to 5.08 at the inflow plane, connects the top and bottom of the duct. Centerline symmetry at $Z = 0$ is assumed, and the flow conditions for the simulation are as follows: $M_\infty = 4.0$, $T_\infty = 89$ K, $T_{\text{wall}} = 248$ K, and $Re/m = 1.07 \times 10^6$. Simulated oil flow patterns along the sidewall and duct bottom, shown in Fig. 9, illustrate the complex flow interactions within the duct. As a result of the low Reynolds number and relatively high wall temperature, thick boundary layers develop on all solid surfaces, displacing the inviscid core flow. The bow shocks generated through displacement effects interact with the developing viscous layers and with the separation shock and compression fan systems emanating from the ramp apex ($X = 7.62$ cm). Lines of coalescence and divergence on the duct bottom show the extent of a pocket of axially separated flow, which reduces in size near the sidewall. Although not clearly indicated, axial separation of the sidewall boundary layer also occurs in the vicinity of the ramp apex-sidewall juncture. The ramp-induced shock systems also separate the sidewall viscous layer in a crossflow manner, producing an upturning of the flow downstream of the ramp apex.

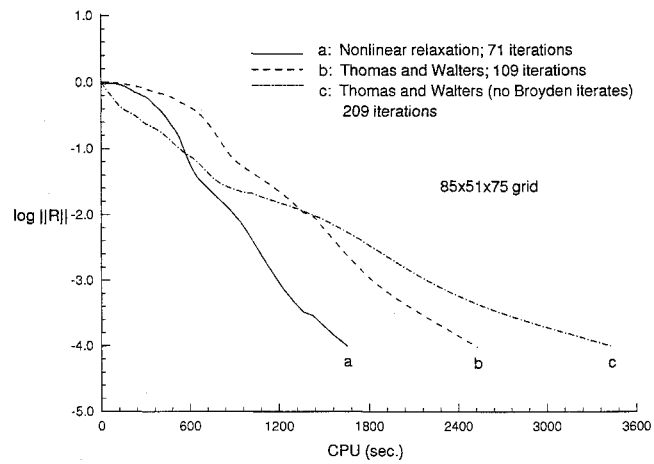

Fig. 8 Convergence histories (Bogdanoff case, 9-deg fin).

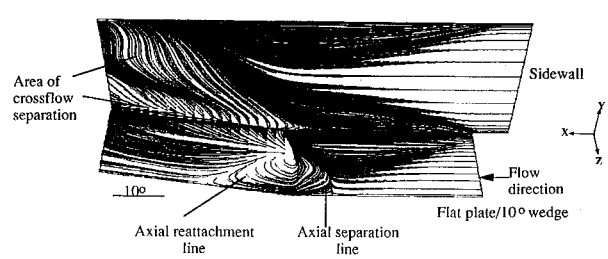

Fig. 9 Simulated oil flow pattern (ramped duct with sidewall).

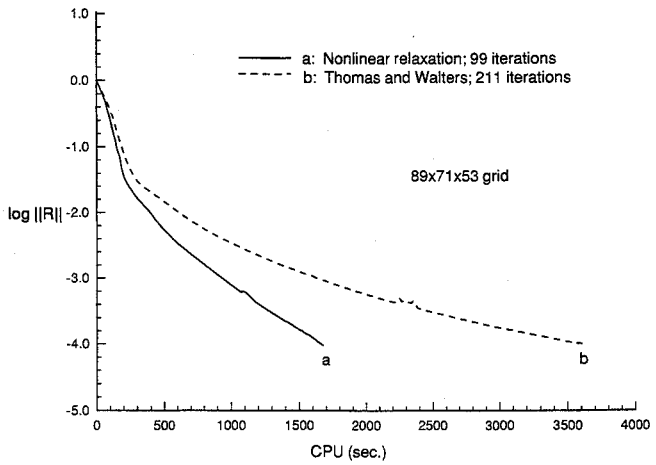

Fig. 10 Convergence histories (ramped duct with sidewall).

Algorithmic parameters for this simulation (performed on an $89 \times 71 \times 53$ grid) are as follows: $\omega_f = \omega_b = 1.0$, initial $\Delta t_0 = 0.02$, final $\Delta t_0 = 0.091$, two Broyden iterates per crossflow plane. As mentioned earlier, the ramped duct configuration contains several regions of axially separated, low Mach number, vortical flow and thus constitutes a severe test for a streamwise-aligned relaxation procedure. The convergence histories in Fig. 10 show that the nonlinear relaxation procedure of Eq. (17) rapidly finds a steady solution, converging in under 28 min of CPU time. The approach of Thomas and Walters requires over 1 h of CPU time to reach the same level of residual reduction. These results confirm the utility of the nonlinear relaxation algorithm in providing rapid convergence for shock-separated flowfields and serve to illustrate the possibilities of the approach for more complex internal flow computations.

Conclusions

The development of an efficient, fully implicit, upwind relaxation Navier-Stokes solver, especially designed to compute three-dimensional high-speed internal flowfields, has been described. Based on a planar Gauss-Seidel iteration strategy, the new algorithm has been shown to provide rapid convergence for the medium-sized (206,000–335,000 mesh points) cases considered. Improvements in time to convergence of 18–54%, compared with respect to a more conventional planar relaxation strategy, have been demonstrated, with the greater improvements obtained for cases containing large pockets of streamwise elliptic flow. A quasi-Newton technique has been used successfully to reduce crossflow matrix factorization errors resulting from an alternating-direction-implicit approximation, thus alleviating much of the numerical stiffness associated with multiple-wall mesh clustering. For the shock-wave/boundary-layer interactions considered in this investigation, a hybrid upwind/central-difference discretization of the governing equations has been shown to yield good comparisons with experimental data when applied in conjunction with a modified form of the Baldwin-Barth turbulence model.

Acknowledgments

This work was supported by the Graduate Training and Research Program in Hypersonic Aerodynamics Grant NAGW-1072, funded jointly by NASA, the Air Force Office of Scientific Research, and Office of Naval Research. Time on the Cray Y-MP was provided by a grant from the North Carolina Supercomputing Center.

References

[1]Thomas, J. L., and Walters, R. W., "Upwind Relaxation Algorithm for the Navier-Stokes Equations," *AIAA Journal,* Vol. 25, No. 4, 1987, pp. 527–534.

[2]Taylor, A. C., Ng, W. F., and Walters, R. W., "Upwind Relaxation Algorithms for the Navier-Stokes Equations Using Inner Iterations," AIAA Paper 89-1954, June 1989.

[3]Newsome, R. K., Walters, R. W., and Thomas, J. L., "An Efficient Iteration Strategy for Upwind/Relaxation Solutions to the Thin-Layer Navier-Stokes Equations," AIAA Paper 87-1113, Jan. 1987.

[4]MacCormack, R. W., "Solution of the Navier-Stokes Equations in Three Dimensions," AIAA Paper 90-1520, June 1990.

[5]Zha, G. C., and Bilgen, E., "An Efficient Upwind Relaxation-Sweeping Algorithm for Three-Dimensional Navier-Stokes Equations," AIAA Paper 92-0023, Jan. 1992.

[6]Thomas, J. L., Van Leer, B., and Walters, R. W., "Implicit Flux-Split Schemes for the Euler Equations," *AIAA Journal,* Vol. 28, No. 6, 1990, pp. 973, 974.

[7]Candler, G. V., and MacCormack, R. W., "Hypersonic Flows Past 3-D Configurations," AIAA Paper 87-0480, Jan. 1987.

[8]Edwards, J. R., and McRae, D. S., "A Nonlinear Relaxation/Quasi-Newton Algorithm for the Compressible Navier-Stokes Equations," AIAA Paper 92-2643, June 1992.

[9]Kim, K., Lee, Y., Alvi, F., Settles, G., and Horstman, C., "Laser Skin Friction Measurements and CFD Comparison of Weak-to-Strong Swept Shock/Boundary Layer Interactions," AIAA Paper 90-0378, Jan. 1990.

[10]Knight, D. D., Horstman, C. C., and Settles, G. S., "Three Dimensional Shock Wave-Turbulent Boundary Layer Interactions Generated by a Sharp Fin at Mach 4," AIAA Paper 91-0648, Jan. 1991.

[11]Batcho, P. F., Ketchum, A. C., Bogdonoff, S. M., and Fernando, E.M., "Preliminary Investigation of the Interactions Caused by Crossing Shock Waves and a Turbulent Boundary Layer," AIAA Paper 89-0359, Jan. 1989.

[12]Bogdanoff, S. M., and Stokes, W. L., "Crossing Shock Wave Turbulent Boundary Layer Interactions—Variable Angle and Shock Generator Length Geometry Effects at Mach 3," AIAA Paper 92-0636, Jan. 1992.

[13]Narayanswami, N., Knight, D. D., Bogdonoff, S. M., and Horstman, C. C., "Crossing Shock Wave-Turbulent Boundary Layer Interactions," AIAA Paper 91-0649, Jan. 1991.

[14]Baldwin, B. S., and Barth, T. J., "A One-Equation Turbulence Transport Model for High Reynolds Number Wall-Bounded Flows," AIAA Paper 91-0610, Jan. 1991.

[15]Tysinger, T. L., and Caughey, D. A., "Implicit Multigrid Algorithm for the Navier-Stokes Equations," AIAA Paper 91-0242, Jan. 1991.

[16]MacCormack, R. W., "Current Status of Numerical Solutions of the Navier-Stokes Equations," AIAA Paper 85-0032, Jan. 1985.

[17]Broyden, C. G., "A Class of Methods for Solving Nonlinear Simultaneous Equations," *Mathematics of Computation,* Vol. 19, 1965, pp. 577–593.

[18]Hager, W. W., "Updating the Inverse of a Matrix," *SIAM Review,* Vol. 31, No. 2, June 1989, pp. 221–239.

[19]Spalart, P. R., and Allmaras, S. R., "A One-Equation Turbulence Model for Aerodynamic Flows," AIAA Paper 92-0439, Jan. 1992.

[20]Cebeci, T., Smith, A. M. O., and Mosinskis, G., "Calculation of Compressible Adiabatic Turbulent Boundary Layers," *AIAA Journal,* Vol. 8, No. 11, 1970, pp. 1974–1982.

[21]Edwards, J. R., "Nonlinear Relaxation Algorithms for the Compressible Navier-Stokes Equations in Two and Three Dimensions," Ph.D. Thesis, Dept. of Mechanical and Aerospace Engineering, North Carolina State Univ., Raleigh, NC, Dec. 1992.